Estimating scale dependence of saturated hydraulic conductivity in soils

by

Skylar Jace Kaminski

B.S., Oklahoma State University, 2020

A THESIS

submitted in partial fulfillment of the requirements for the degree

MASTER OF SCIENCE

Department of Geology
College of Arts and Sciences

KANSAS STATE UNIVERSITY
Manhattan, Kansas

2022

Approved by:

Major Professor
Behzad Ghanbarian

Copyright

Abstract

Understanding the effect of scale on hydraulic and physical properties of soils has broad applications to scaling problems in hydrogeology, soil physics, and environmental engineering. The scale dependence of flow and transport is attributed to spatial heterogeneities, such as pore-size distribution and pore connectivity at small scales (e.g., core), fracture orientation and long-range correlations at large scales (e.g., field). In this study, we apply concepts from percolation theory to estimate the scale dependence of saturated hydraulic conductivity, K_{sat}. For this purpose, we use a database including undisturbed soil samples from four Danish sites (Jyndevad, Tylstrup, Estrup, and Silstrup). The value of K_{sat} was measured at small (100 cm^3) and large (6280 cm^3) scales. First, we apply a classification approach, widely used in petroleum engineering, to group soils based on their similarities in hydraulic properties using porosity and K_{sat} measurements at the small scale. We detect nine different soil classes with the average flow zone indicator (FZI) from 0.05 μm in class 1 to 9 μm in class 9. Next, using percolation theory, we characterize the scale dependence of critical pore-throat radius. We use the critical path analysis to link the critical pore-throat radius to K_{sat} and, consequently, determine the scale dependence of K_{sat}. Comparing the theoretical estimations with the experimental measurements show that the percolation theoretic model reasonably well estimates the K_{sat} at the large scale from the soil water retention curve and K_{sat} measured at the small scale. We find the root mean square log-transformed error (RMSLE) values 0.45, 0.77, 1.9, and 2.05 (cm/day) for sites Jyndevad, Tylstrup, Silstrup, and Estrup, respectively. Results show that the theory tends to provide more accurate estimations in coarser textures and unstructured soils as well as soil classes with FZI values greater than 0.7 μm.

Table of Contents

List of Figures

List of Tables

Acknowledgements

I would like to express my deepest appreciation to my advisor Dr. Behzad Ghanbarian. Not only for his wisdom and help these two years, but for always pushing me to be a better graduate student. I would also like to thank my committee members, Dr. Stacey Kulesza, Dr. Matt Kirk, and Dr. Weston Koehn for the unconditional support, wisdom, and funding. A special thank you is owed to Dr. Andres Patrignani and Dr. Nathanial Parker for teaching and trusting me with some of the lab equipment used for this research. I would also like to thank Dr. Bo Iversen for his advice, and for providing us with his database. Lastly, I would acknowledge and thank the Kansas State University Department of Geology, my peers, and my family for their financial and emotional support.

Chapter 1 - Introduction

Understanding flow and transport in porous media has been an active subject of research due to broad applications in science and industry, particularly contaminated site remediation and wastewater disposal. Fluid flow and solute migration in field, such as groundwater discharge, transmissivity and dispersion, may be studied at different scales e.g., from a few meters to several kilometers. However, field measurements are typically time consuming and expensive. Thus, scaling analyses and more specifically upscaling techniques are required to estimate one property at a larger scale from characteristics available at a smaller scale (Hopmans et al., 2002). For this purpose, one needs to understand the effect of scale on flow and transport. For instance, the scale dependence of dispersion (De Smedt et al., 1986; Pachepsky and Hill, 2017; Gao et al., 2012; Younes et al., 2020), tortuosity (Ghanbarian et al., 2013; Ghanbarian, 2022a; Matyka et al., 2008), and hydraulic conductivity (Lauren et al., 1988; Guimerà et al., 1995; Schulze-Makuch et al., 1999; Hunt, 2006; Fallico et al., 2012; Ghanbarian, 2022b) have been investigated at various scales. However, accurate estimations of soil physical and hydraulic parameters at a larger scale from soil properties available at a smaller scale is still a great challenge.

The scale dependence of hydraulic conductivity has traditionally been investigated in subsurface hydrology at large scales using pumping tests (Garbesi et al., 1996; Javaux and Vanclooster, 2006; Sánchez-Vila et al., 1996; Schulze-Makuch, 1996; Schulze-Makuch et al., 1999). Such studies show that hydraulic conductivity increases with scale. For instance, Schulze-Makuch et al. (1999) proposed the following power-law relationship

$$K_{sat} = aV_s^b \tag{1}$$

where V_s is the sample volume, K_{sat} is the saturated hydraulic conductivity, and a and b are empirical parameters. Although widely used by soil scientists and hydrologists to link K_{sat} to

sample volume or scale (Zota et al., 2009; Fallico et al., 2010; Pachepsky et al., 2014; Brunetti et al., 2022), Eq. (1) is purely empirical (Fallico et al., 2012).

Numerical simulations have also been used to detect the representative elementary volume (REV) of a domain and to study the effect of scale (Aslannejad et al., 2017; Esmaeilpour, 2021; Mostaghimi et al., 2013; Sahimi et al., 1986). REV is the smallest domain size above which physical or hydraulic properties do not change with scale (Bear and Braester, 1972). Mostaghimi et al. (2013) investigated the REV for consolidated and unconsolidated porous media by numerically calculating specific surface area, K_{sat}, and porosity using micro-CT images of different sizes. They showed that the REV value for porosity and specific surface area was different than K_{sat}. Mostaghimi et al. (2013) demonstrated that the K_{sat} REV could be up to two times greater than the porosity and specific surface area REV. Recently, Esmaeilpour et al. (2021) investigated the effect of scale on both hydraulic and electrical conductivities using pore-scale simulations. They found that both hydraulic and electrical conductivities increased as domain size increased. Ghanbarian et al. (2021), however, demonstrated that depending on pore coordination number, hydraulic conductivity may increase or decrease with scale using pore network simulations.

Ghanbarian et al. (2015) applied a machine learning method called contrast pattern aided regression and developed scale-dependent pedotransfer functions to estimate soil water retention curve (SWRC) and K_{sat} using soil samples from the UNSODA database. By including sample diameter and length as input variables, they showed that the accuracy of scale-dependent pedotransfer functions was higher than those developed without those that incorporate sample dimensions. Using a large database of nearly 20000 samples, Ghanbarian et al. (2017) demonstrated that scale-dependent pedotransfer functions developed by Ghanbarian et al. (2015)

estimated K_{sat} substantially more accurately than several other models widely used in the literature.

Within the critical path analysis framework, K_{sat} depends on some critical pore-throat radius and electrical conductivity (Katz and Thompson, 1986; Ghanbarian, 2020). By applying the critical path analysis approach and assuming that K_{sat} is dominantly controlled by critical pore-throat radius (Hunt, 2006), Esmaeilpour et al. (2021) proposed Eq. (2) to explain the scale dependence of hydraulic conductivity as follows:

$$K_{sat}(L) = K_{sat}(L_{min}) \left[\frac{r_{tc}(L)}{r_{tc}(L_{min})}\right]^2 \tag{2}$$

where $K(L)$ is the scale-dependent saturated hydraulic conductivity, $K(L_{min})$ is the K_{sat} at the smallest scale, $r_{tc}(L)$ is critical pore-throat radius at the large scale, and $r_{tc}(L_{min})$ is critical pore-throat radius at the smallest scale. Eq. (2) ignoring the effect of electrical conductivity on K_{sat} may be applied when electrical conductivity data are not available.

By comparing with pore-network simulations, Esmaeilpour et al. (2021) showed that Eq. (2) estimated the scale dependence of permeability with high accuracy. They reported the relative error ranged from -3.7% to 0.74%.

Although the performance of Eq. (2) was evaluated by Esmaeilpour et al. (2021) using pore-scale simulations, it has not yet been assessed with experimental measurements and agricultural soils, which are complex systems (Minasny et al., 2008). Therefore, the main objective of this study is to evaluate the accuracy of Eq. (2) using a database of agricultural soil samples from four sites and different horizons.

Chapter 2 - Theory

Percolation theory addresses flow and transport in a network of pores through scaling relationships by taking the effect of interconnectivity into account (Sahimi, 2011; Hunt et al., 2014). Although initial percolation-based models were developed based on bond and site percolation classes and regular networks, more realistic and representative models were later proposed using irregular and disordered systems (Tyč and Halperin, 1989; Kogut and Straley, 1979). Esmaeilpour et al. (2021) generalized the methodology originally proposed by Hunt (2006) to link the scale dependence of K_{sat} to the scale dependence of critical pore-throat radius. Using concepts of percolation theory, Esmaeilpour et al. (2021) derived

$$f_c = \frac{\int_{r_{tc}}^{r_{tmax}} l_t r_t^2 f(r_t) dr_t}{\int_{r_{tmin}}^{r_{tmax}} l_t r_t^2 f(r_t) dr_t} \tag{3}$$

where f_c is the critical volume fraction of pores, $f(r_t)$ is the pore-throat radius distribution, r_{tmin} and r_{tmax} are respectively the minimum and maximum pore-throat radii, l_t is the pore-throat length, and r_{tc} is the critical pore-throat radius.

Esmaeilpour et al. (2021) related the critical pore-throat radius to the pore-throat radius distribution, $f(r_t)$, typical pore-throat length, l_{t0}, and the system size, L, as follows

$$\frac{\int_{r_{tc}}^{r_{tmax}} l_t r_t^2 f(r_t) dr_t}{\int_{r_{tmin}}^{r_{tmax}} l_t r_t^2 f(r_t) dr_t} = \left(\frac{l_{t0}}{L+l_{t0}}\right)^{\frac{1}{v}} \tag{4}$$

which implicitly explains the scale dependence of r_{tc}. As L increases, the ratio $(l_{t0}/(L + l_{t0}))^{\frac{1}{v}}$ decreases, if l_{t0} remains constant. Accordingly, r_{tc}, as the lower limit of the integral, has to increase, if $f(r_t)$ does not vary with the scale. v in Eq. (4) is a universal scaling exponent whose value is 0.88 in three dimensions (Hunt et al., 2014). Based on Eq. (4), the larger the system size, the greater the r_{tc}, if $f(r_t)$ and l_{t0} remain scale-invariant. This agrees with the results of Koestel

et al. (2020) who showed that as system size increased, the value of r_{tc} increased following a nonlinear trend.

Chapter 3 - Materials and Methods

3.1 -Experiments

The data used in this study are from a database of 196 soil samples from four sites (i.e., Jyndevad, Tylstrup, Estrup, and Silstrup) in Denmark published by Iversen et al. (2001). The samples, collected at two to three soil profiles by coring, are agricultural soils that range from sand to loam in texture according to Soil Survey Division Staff (1993). Table 3.1 summarizes the salient properties of the samples at each site. The large-scale samples were collected using a 6280 cm^3 (inner diameter 20 cm) hydraulic press core. The small-scale samples were collected using a 100 cm^3 (inner diameter 6.1 cm) core that was driven into the soil. All samples were protected from evaporation and physical disruption and stored at 2–5° C until experimental measurements commenced (Iversen et al., 2001).

At the small scale (100 cm^3), soil samples were back saturated and then placed on top of a sandbox to measure the SWRC at tension heads h = 10, 16, 50, and 100 cm H$_2$O. The pressure plate method was then used at h = 160 and 1000 cm H$_2$O. The SWRC at h = 15850 cm H$_2$O was measured on disturbed samples after grinding and sieving through a 2-mm sieve. After that, the samples were re-saturated for at least 24 hours, and then the K_{sat} was measured using the constant head method and the Darcy equation (Klute and Dirksen,1986). At the large scale (6280 cm^3), K_{sat} was measured using the constant head method suggested by Klute and Dirksen (1986).

Table 3.1 Some properties of the soil samples used in this study (Iversen et al., 2001).

Site	Horizon	Depth (cm)	Clay (%) < 2 μm	Silt (%) 2-20 μm	Sand (%) 20-2000 μm	Soil texture	Organic matter (%)	Bulk density (g/cm³)
Jyndevad	Ap	0–32	5.4	3.1	91.5	sand	2.9	1.40
	Bhs/Bs	32–45	5.2	1.9	93	sand	1.6	1.45
	BC/C	92–135	6.5	0.7	92.8	sand	0.2	1.50
Tylstrup	Ap	0–32	5.9	4.4	89.7	sand	2.7	1.39
	Bv/Ap2	32–72	4.8	4.4	90.9	sand	1.4	1.40
	BC/C	87–155	3.1	0.9	96	sand	0.2	1.40
Silstrup	Ap	0–31	22.1	16.4	61.5	sandy clay loam	3.1	1.48
	Bv	31–70	29.2	14.1	56.7	sandy clay loam	0.5	1.61
	BC(g)/C	115–146	24.5	14.0	61.4	sandy clay loam	0.1	1.75
Estrup	Ap	0–27	15.2	12.1	72.7	sandy loam	4.1	1.51
	BE(g)/Bhs/Bt(g)	27–52	19.1	8.5	72.4	sandy loam	0.6	1.69
	Cg/C	117–168	33.1	22.8	44.1	clay loam	0.2	1.64

3.2 -Classifying Soils

In this section, we present the theory of soils classification based on porosity and K_{sat} data measured at the small scale. For this purpose, we first invoke the approach proposed by Amaefule et al. (1993), widely applied in petroleum engineering to group rocks in sandstone (Bhattacharya et al., 2008) and carbonate (Martin et al., 1997) reservoirs, and then adopt it for soils.

Amaefule et al. (1993) used the concept of mean hydraulic radius to modify the Kozeny-Carman model and generalized it as follows:

$$k = \frac{\phi^3}{(1-\phi)^2} \left[\frac{1}{F_s \tau^2 S_{gv}^2}\right] \qquad (5)$$

where k is the permeability (μm^2), ϕ is the porosity (cm^3/cm^3), F_s is a shape factor (= 2 for a circular cylinder), τ is the tortuosity (> 1), and S_{gv} is the surface area per unit grain volume ($1/\mu m$).

Amaefule et al. (1993) divided both sides of Eq. (5) by porosity and took the square root to have

$$\sqrt{\frac{k}{\phi}} = \frac{\phi}{1-\phi}\left[\frac{1}{\sqrt{F_s\tau}S_{gv}}\right] \tag{6}$$

Those authors then defined $\sqrt{\frac{k}{\phi}}$ as the quality index (hereafter SQI, soil quality index). The concept of SQI is similar to that of average linear velocity widely used in groundwater literature (Freeze and Cherry, 1979). Since normalized porosity ϕ_z, the pore volume-to-grain volume ratio (also known as void ratio), is $\frac{\phi}{(1-\phi)}$, Eq. (6) can be rewritten as

$$SQI = \phi_z FZI \tag{7}$$

in which $FZI = \frac{1}{\sqrt{F_s\tau}S_{gv}}$ is called the flow zone indicator.

Amaefule et al. (1993) proposed plotting the SQI against the ϕ_z to identify different types or classes. Based on their terminology, samples that lie on a straight line with a unit slope would correspond to the same hydraulic flow unit and group. Each hydraulic flow unit is characterized with a unique FZI value, which is the intercept of the unit-slope line with $\phi_z = 1$.
To classify soils from four different sites, we determined soil permeability from dividing small-scale K_{sat} by fluidity factor. Then, the SQI value was calculated from soil porosity and permeability both measured at the small scale. The value of ϕ_z was also determined from porosity measurement at the small scale. By plotting the SQI against the ϕ_z, we draw lines with unit slopes using different FZI values and captured soil samples belonged to the same trend.

3.3 -Estimating Large-Scale K$_{sat}$

Since the soil water retention data were not available at the large scale, we assumed that

the pore-throat radius distribution, $f(r_t)$, does not change with the scale. To determine the scale

dependence of r_{tc} via Eq. (4), we first calculated the value of r_{tc} at the smaller scale using the

SWRC by setting f_c equal to $\theta(h = 15450\ cm)/\theta_s$ and solving Eq. (3) numerically. For this

purpose, the $f(r_t)$ was determined from the SWRC measurements and by fitting the van

Genuchten (1980) model to the data

$$\theta = (\theta_s - \theta_r)[1 + (\alpha h)^n]^{-m} + \theta_r \tag{8}$$

where θ_s and θ_r are the saturated and residual volumetric water contents, respectively, h is the

tension head, and α, n, and m are shape parameters. We fitted Eq. (8) directly to the measured

SWRCs using the nonlinear least square approach in MATLAB and optimized the values of α,

n, m, and θ_r simultaneously. For this purpose, we considered n and m as two independent fitting

parameters. For the sake of higher flexibility, we also let the parameter n to be less than 1 and m

greater than 1.

After optimizing the van Genuchten (1980) shape parameters, the pore-throat radius

distribution was calculated as (Dexter, 2004)

$$f(r_t) = mn(\theta_s - \theta_r)\left(\frac{0.149\alpha}{r}\right)^n \left[1 + \left(\frac{0.149\alpha}{r}\right)^n\right]^{-m-1} \tag{9}$$

where all variables have previously been defined. The typical pore-throat length, l_{t0}, was not

known in our samples. We, therefore, estimated its value for each sample via Eq. (4) from r_{tc}

and $f(r_t)$ determined at the small scale. We also assumed that l_{t0} does not change with the scale,

and the optimized value of l_{t0} was used to determine the r_{tc} at the large scale via Eq. (4). Pore-

throat lengths and their distribution are not typically measured in soil surveys. Since such

information were not known for the soil samples studied here, we treated l_t in Eq. (4) as a constant and canceled it out.

After calculating the values of r_{tc} at the small and large scales, we used Eq. (2) to estimate the large scale K_{sat} from the small scale one. To evaluate the predictability of Eq. (2), we calculated the root mean square log-transformed error as follows:

$$RMSLE = \sqrt{\frac{1}{N}\sum_{i=1}^{N}[\log(x_{est}) - \log(x_{meas})]^2} \qquad (10)$$

where N is the number of samples, x_{est} is the estimated K_{sat}, and x_{meas} is the measured value.

Chapter 4 - Results and Discussion

The average values of the fitted van Genuchten (1980) model parameters and their standard deviations are presented in Table 4.1. We found the average θ_s and n values for the Silstrup and Estrup sites smaller than the Jyndevad and Tylstrup sites. More specifically, the average value of n for the Estrup site was 0.55. Although $n > 1$ is typically reported in literature, our results are consistent with those estimated by Zakizadeh Abkenar and Rasoulzadeh (2019). They found n to be 0.73 and 0.63 in a loamy and a clay loamy soil sample, respectively. As discussed by van Genuchten and Nielsen (1986), one may expect n values less than 1 when m and n are considered to be independent variables, particularly in structured and/or coarse-textured soils. In our study, we also found $n < 1$ for sandy loam and clay loam samples in the Estrup site (Table 3.1). Since empirical parameters n and m are independent fitting parameters in our study and the purpose of fitting the van Genuchten SWRC model to the data was deriving a continuous form of the $f(r_t)$, we do not expect n values less than 1 impact the obtained results.

Table 4.1 The average values of the optimized parameters of the van Genuchten (1980) soil water retention curve model, Eq. (5), reported for each site studied here. Numbers in parentheses represent the standard deviations.

Site	van Genuchten (1980) model parameters				
	θ_s (cm³/cm³)	θ_r (cm³/cm³)	α (1/cm)	n (-)	m (-)
Jyndevad	0.461 (0.025)	3.9×10^{-4} (0.003)	0.121 (0.043)	4.065 (7.38)	0.258 (0.20)
Tylstrup	0.469 (0.038)	0.011 (0.012)	0.039 (0.025)	15.97 (20.67)	0.219 (0.24)
Silstrup	0.390 (0.052)	0.023 (0.014)	0.172 (0.855)	1.00 (0.003)	0.219 (0.13)
Estrup	0.407 (0.052)	0.011 (0.009)	2.06×10^{-6} (5.3×10^{-6})	0.55 (0.31)	26.16 (15.65)

The average values of α were 0.121, 0.039, 0.172, and 2.06×10^{-6} cm^{-1} for the Jyndevad, Tylstrup, Silstrup, and Estrup sites, respectively (Table 3.1). We found similar average α values for the Jyndevad and Silstrup sites, although the two sites have different soil textures (sand versus sandy clay loam). Generally speaking, the samples from the Silstrup site are finer in texture compared to Jyndevad. We should note that α is inversely proportional to the air entry tension head, a parameter that is affected by soil structure more than its texture, particularly in undisturbed samples (Ghanbarian-Alavijeh et al., 2010).

Fig. 4.1 presents the volumetric water content versus the tension head as well as the K_{sat} against the porosity for the soil samples in each site at the small scale (100 cm^3). Recall that the SWRC data were only available at the small scale. As can be seen, the volumetric water contents measured at 15540 cm H$_2$O are greater in the Silstrup (Fig. 4.1c) and Estrup (Fig. 4.1d) samples compared to Jyndevad (Fig. 4.1a) and Tylstrup (Fig. 4.1b). This indicates the soils from Silstrup and Estrup are finer in texture compared to those from Jyndevad and Tylstrup. This is consistent with the soil textures reported from the different horizons in Table 3.1.

Comparing the $\phi - K_{sat}$ in Figs. 4.1e-h shows that the small scale K_{sat} for soil samples from the Jyndevad site (Fig. 4.1e) is greater than the other sites. Although the $\phi - K_{sat}$ data in the Jyndevad site are scattered, the data from other sites exhibit an increasing trend. The value of porosity in the Jyndevad and Tylstrup sites is typically limited between 0.4 and 0.55 cm^3/cm^3. However, soil samples from the Silstrup and Estrup sites have a broader range of porosity ($0.3 < \phi < 0.5$).
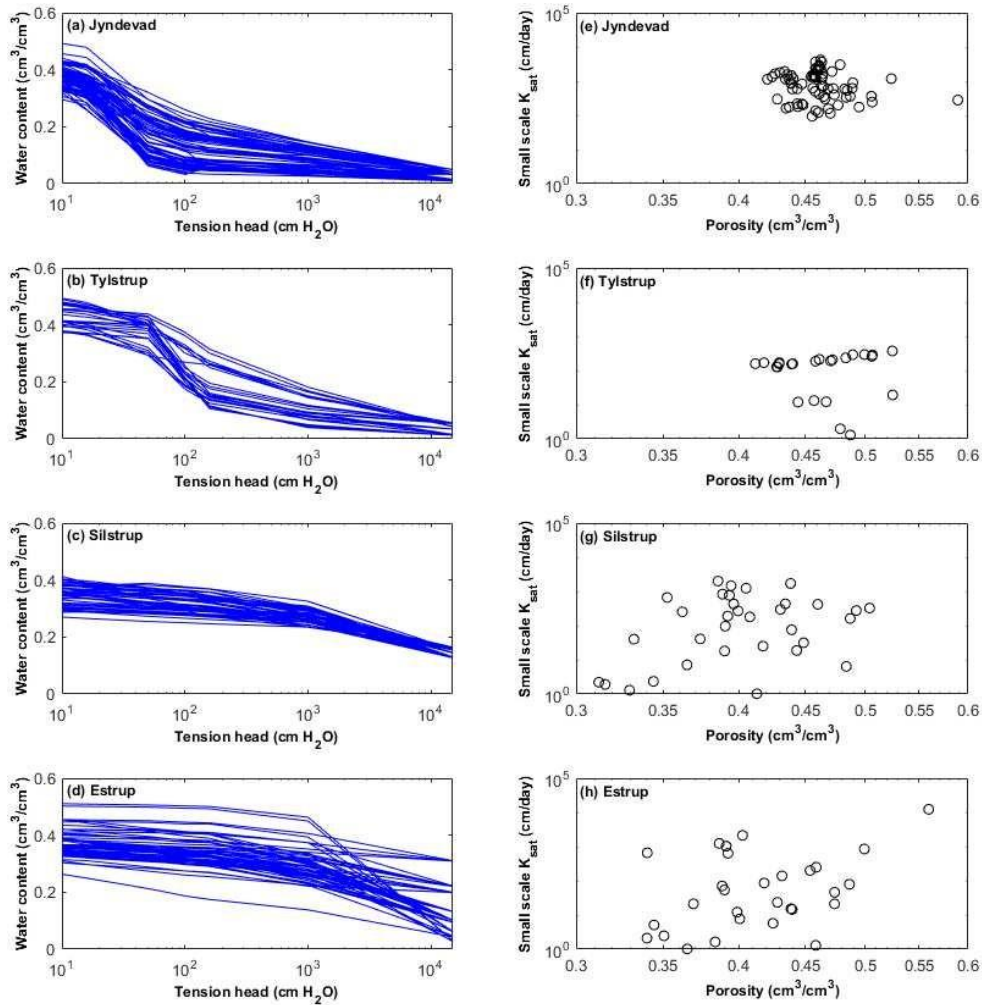
Figure 4.1 Volumetric water content against tension head and saturated hydraulic conductivity versus porosity measured at small scale for the soils in the Jyndevad (73 samples), Tylstrup (25 samples), Silstrup (45 samples), and Estrup (53 samples) sites.

Fig. 4.2 shows the histogram of natural logarithm of K_{sat} measured at the small (left column) and large (right column) scales for the soil samples from the four sites. Literature supports that the histogram of $\ln(K_{sat})$ may approximately follow the Gaussian (Jiménez-Aguirre et al., 2018; Adeyemi et al., 2022) or Stable (Molz et al., 2004) distribution. However, some histograms shown in Fig. 4.2 display bimodal behavior and some others do not seem to follow a

specific type of probability density function (Figs. 4.2c and 4.2g). This is likely because the number of soil samples from each site is limited. Godoy et al. (2019) analyzed fifty soil samples and also found that $\ln(K_{sat})$ did not conform to the Gaussian distribution. Results presented in Fig. 4.2 show that the histograms at the small scales are different from those at the large scale, which indicates the effect of scale (Bear and Braester, 1972). The histograms from one site are also different than those from another site, which is due to spatial heterogeneities, particularly differences in soil textural and structural characteristics. Recall that soil samples from the Jyndevad and Tylstrup sites are sandy, while those from Estrup and Silstrup are loamy and more structured (Iversen et al., 2001)
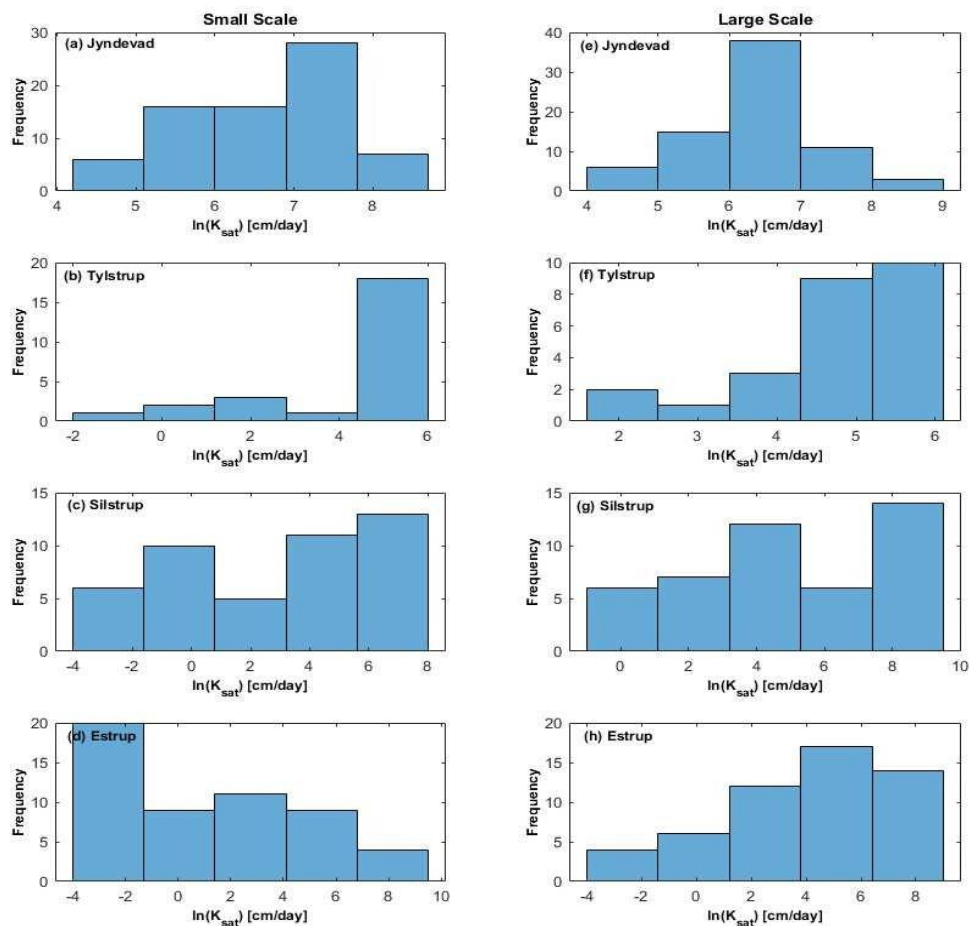
Figure 4.2 The histogram of natural logarithm of K_{sat} for small (left column) and large (right column) scales. The number of samples in the Jyndevad, Tylstrup, Silstrup, and Estrup sites are 73, 25, 45, and 53, respectively.

4.1 -Soil Classes

Soil classification results based on the Amaefule et al. (1993) approach are presented in Fig. 4.3a. We detected nine soil classes each of which is characterized by a different average FZI value. We found that the FZI values spanned over two orders of magnitude in variation from 0.05 to 9 μm (Table 4.2), which indicates substantially different soil hydraulic properties within the soil database studied here. As reported in Table 4.2, classes 4 and 9 are the smallest and largest groups with respectively 5 and 48 soil samples. We found that soils with higher FZIs ($\geq$ 2.35 μm) were more frequent in the database analyzed in this study. This can also be inferred from Fig. 4.3a showing that the majority of samples have SQI > 0.6 μm.

The FZI is a parameter that differentiates pore geometrical facies based on soil texture and mineralogy (Amaefule et al., 1993). Soil samples in classes with greater FZIs (e.g., classes 8 and 9) incorporate larger pore throats in general. Fig. 4.3b displays the distribution of soil classes in each site. We found that the Jyndevad and Tylstrup sites included samples from four and five classes, respectively, were the least diverse sites. In contrast, the Silstrup and Estrup sites were the most diverse ones contained soil samples from all nine classes detected. This is well in accord with the fact that the loamy soils from Silstrup and Estrup are more structured than those from Jyndevad and Tylstrup.
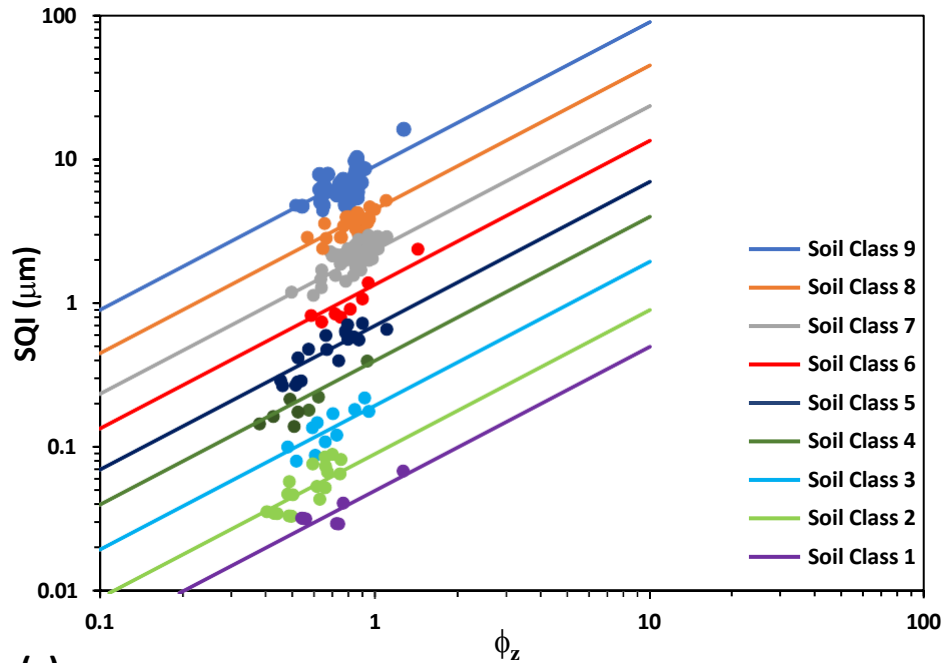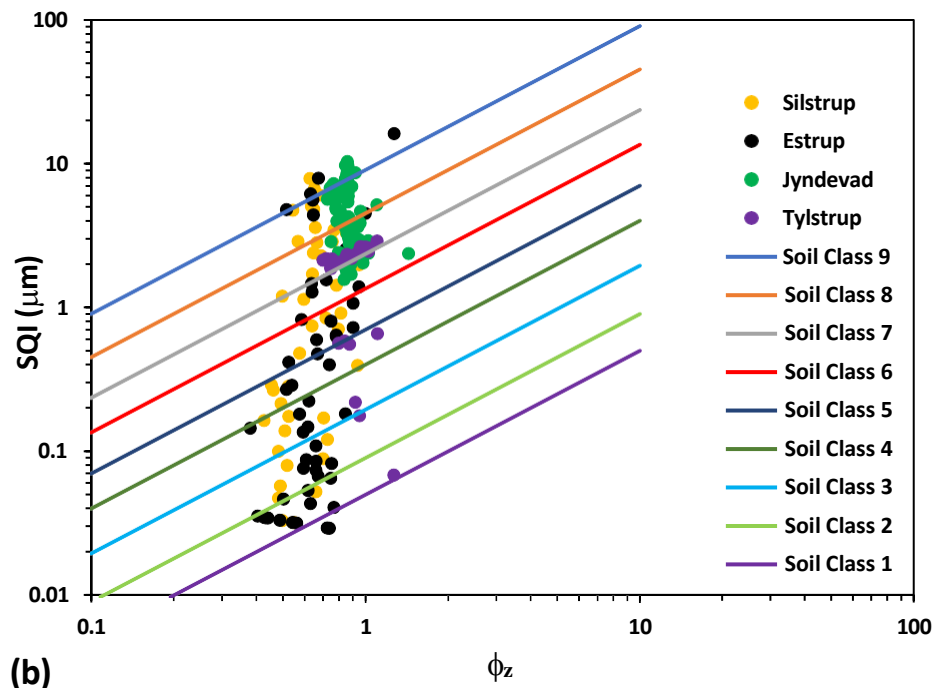
Figure 4.3 Soil quality index against normalized porosity for 196 soil samples studied here. (a) shows nine different soil classes found using the Amaefule et al. (1993) approach, and (b) present the distribution of soil classes in each site.

Table 4.2 The nine soil classes with different average FZI values detected using the Amaefule et al. (1993) approach.

Soil class	No. of samples	Ave. FZI (μm)
1	7	0.05
2	18	0.09
3	15	0.20
4	5	0.40
5	18	0.70
6	8	1.35
7	45	2.35
8	32	4.50
9	48	9.00

We should note that using the Amaefule et al. (1993) approach one should expect unstructured/coarse-textured and structured/fine-textured soils with similar permeability and porosity values to be grouped into the same soil class. However, even if their permeabilities are similar, an unstructured/coarse-textured soil typically has a lower porosity compared to a structured/fine-textured soil. This means their ϕ_z values might be different and so their soil classes.

4.2 -Large-Scale K_{sat} Estimations

Table 4.3 summarizes values used to estimate the large-scale K_{sat}. The average values of minimum and maximum pore-throat radii (r_{tmin} and r_{tmax}) were determined respectively from the maximum and minimum tension heads using the Young-Laplace equation (assuming zero contact angle) and the measured SWRC. The r_{tc} values were calculated at the small and large scales. As can be seen, the average r_{tc} at the large scale is greater than that at the small scale (Table 4.3).

Table 4.3 The average values of minimum and maximum pore-throat radii (r_tmin and r_tmax) determined from maximum and minimum tension heads and the measured SWRC, critical pore-throat radius (r_tc) at the small scale computed by setting $\boldsymbol{f_c}$ equal to $\boldsymbol{\theta}(\boldsymbol{h} = 15450\ \boldsymbol{cm})/\boldsymbol{\theta}_s$ and solving Eq. (3) numerically, and critical pore-throat radii (r_tc) at the large scale computed by solving Eq. (4). Numbers in parentheses represent the standard deviations.

Site	r_tmin (cm)	r_tmax (cm)	small scale r_tc (cm)	large scale r_tc (cm)
Jyndevad	9.4013×10^{-6} (-)	0.0149 (-)	0.0146 (7.24×10^{-4})	0.0148 (6.26×10^{-4})
Tylstrup	9.4013×10^{-6} (-)	0.0149 (-)	0.0109 (0.0046)	0.0116 (0.0047)
Siltrup	9.4013×10^{-6} (-)	0.0149 (-)	0.0112 (7.90×10^{-4})	0.0138 (3.40×10^{-4})
Estrup	9.4013×10^{-6} (-)	0.0149 (-)	0.0122 (0.0017)	0.0140 (8.17×10^{-4})

The estimated K_{sat} values at the large scale against the measured ones are presented in Fig. 4.4 for samples in the Jyndevad site. We found the RMSLE value of 0.45 with most large-scale K_{sat} estimations around the 1:1 line. The proposed model estimated the large-scale K_{sat} reasonably well for all samples except three (all from class 7) for which the K_{sat} was underestimated by more than one order of magnitude. In structured soil samples, such a great difference between theory and experiment may be attributed to the presence of macropores (Jarvis, 2008; Iversen et al., 2012) that are not captured by the SWRC. However, by means of computed tomography imaging one should be able to characterize soil structures and quantify macropores (Heijs et al., 1995; Elliot et al., 2010; Bölscher et al., 2021). Most samples from the Jyndevad site are unstructured and sandy with low organic contents (Iversen et al., 2001). However, those three samples from class 7 are from the Ap horizon (depth 0-32 cm) with high organic matter (Table 3.1). This means they might be weakly structured with some macropores present.
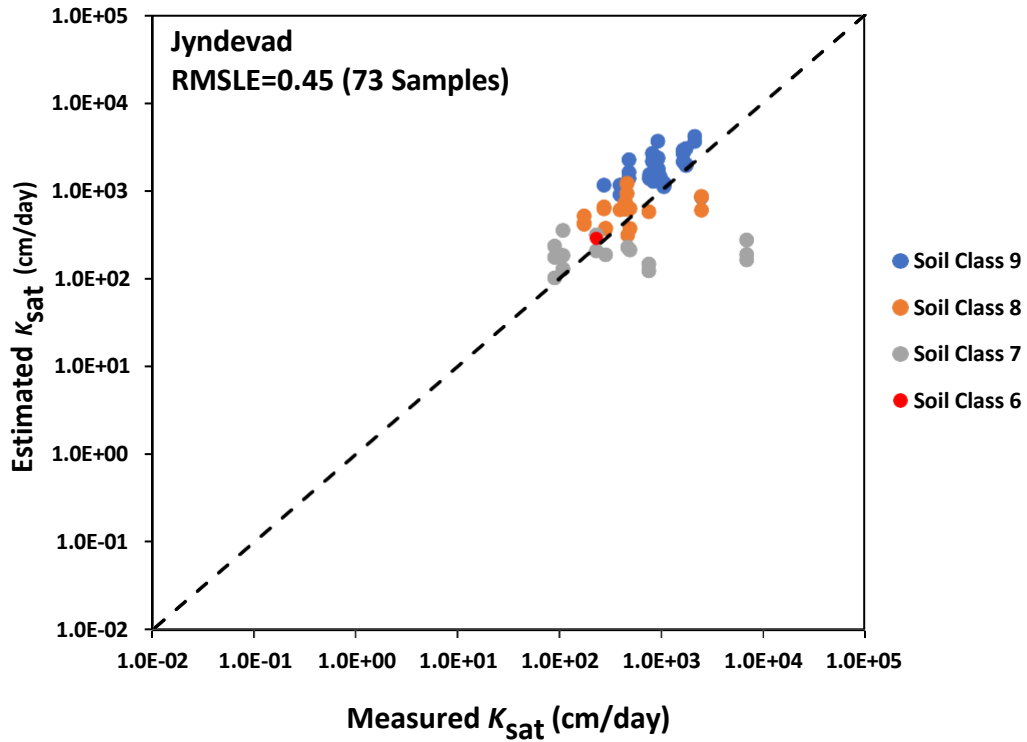
Figure 4.4 The estimated saturated hydraulic conductivity at the large scale against the measured one for samples in the Jyndevad site. The solid line indicates the 1:1 line.

Fig. 4.5 shows the estimated large-scale K_{sat} versus the measured one for samples from the Tylstrup site with RMSLE = 0.77 (cm/day). Similar to Fig. 4, the proposed model estimated the large-scale K_{sat} for most samples with good accuracy. However, for three samples the underestimation is substantial. For these three samples belonging to classes 1, 3, and 5 (Fig. 4.5), we found that the average ratio of large-scale K_{sat} to small-scale K_{sat} was 171.6. This means that the large-scale K_{sat} was, on average, more than two orders of magnitude greater than the small-scale K_{sat}. Interestingly, the average ratio for other samples from the Tylstrup site was 1.12. Given that those three samples are from the Ap horizon (depth 0-32 cm) with high organic matter (Table 3.1), such a substantial difference in small- and large-scale K_{sat} values may be

18

attributed to the presence of macropores, as discussed above. By removing those three samples from the calculations, the value of RMSLE reduced from 0.77 to 0.31 cm/day.
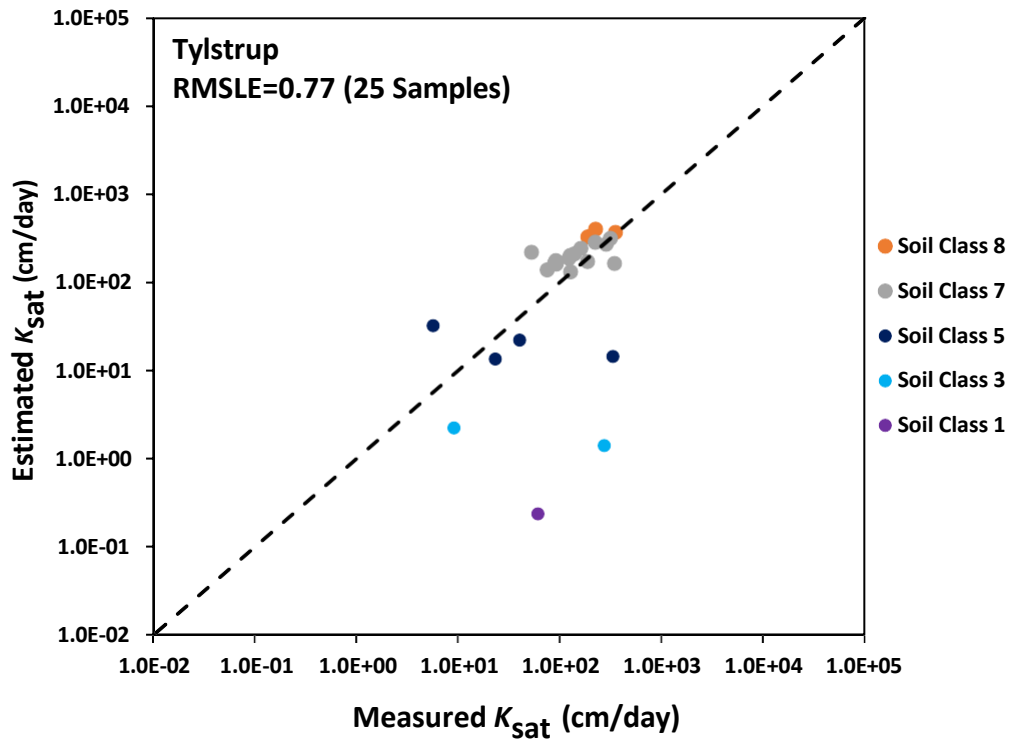
Figure 4.5 The estimated saturated hydraulic conductivity at the large scale against the measured one for samples in the Tylstrup site. The solid line indicates the 1:1 line.

The large-scale estimations of K_{sat} for soils from the Silstrup site are shown in Fig. 4.6. Although for some soil samples the proposed model overestimated the large-scale K_{sat}, results indicate that its value was mainly underestimated in this site. This is most probably because the soil samples from the Silstrup site are loamy and structured (Iversen et al., 2001), and, thus, one may expect macropores to be present, as discussed above. We found the RMSLE value of 1.9 cm/day, which is nearly four times greater than that in Jyndevad and three times greater than that in Tylstrup. Similar results were obtained for the Estrup site (Fig. 4.7). The Silstrup and Estrup

sites are the most diverse sites with samples from all nine soil classes detected. Although the estimations plots look scattered for the Silstrup and Estrup sites (with finer soil textures) as shown in Figs. 4.6 and 4.7, we generally found that the proposed model estimated the large-scale K_{sat} in classes with greater FZIs (e.g., classes 7, 8, and 9) more accurately. Similar results were obtained for the Jyndevad and Tylstrup sites for which most estimations presented in Figs. 4.4 and 4.5 seem to be around the 1:1 line. In what follows, we discuss in more details some potential sources that may have caused K_{sat} underestimation.
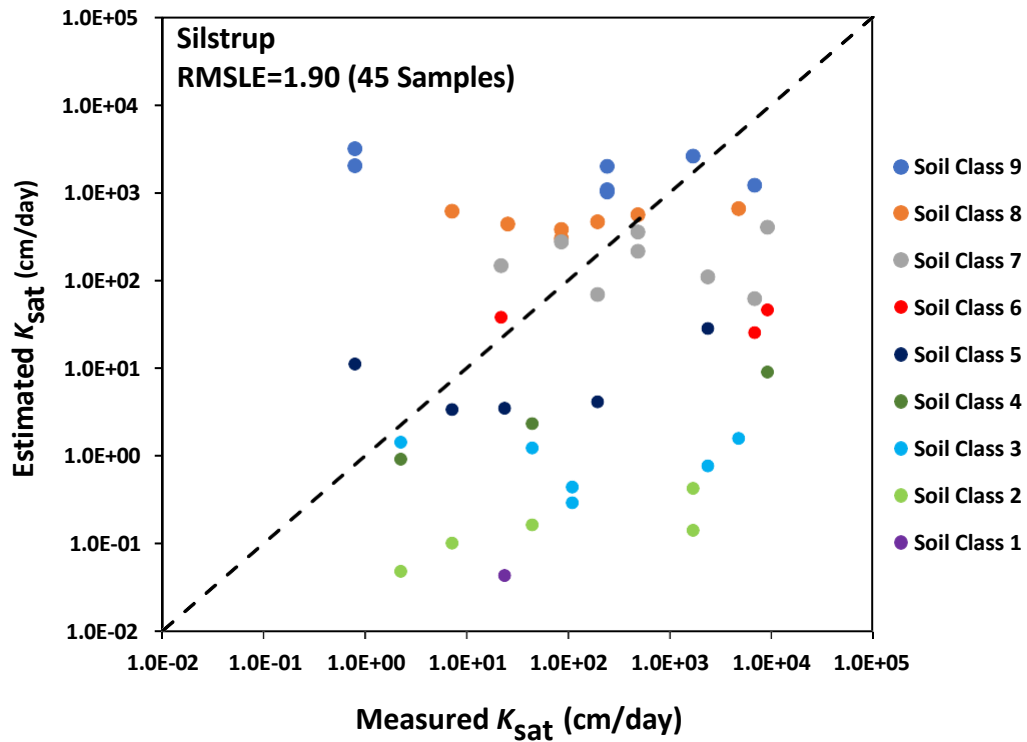
Figure 4.6 The estimated saturated hydraulic conductivity at the large scale against the measured one for samples in the Silstrup site. The solid line indicates the 1:1 line
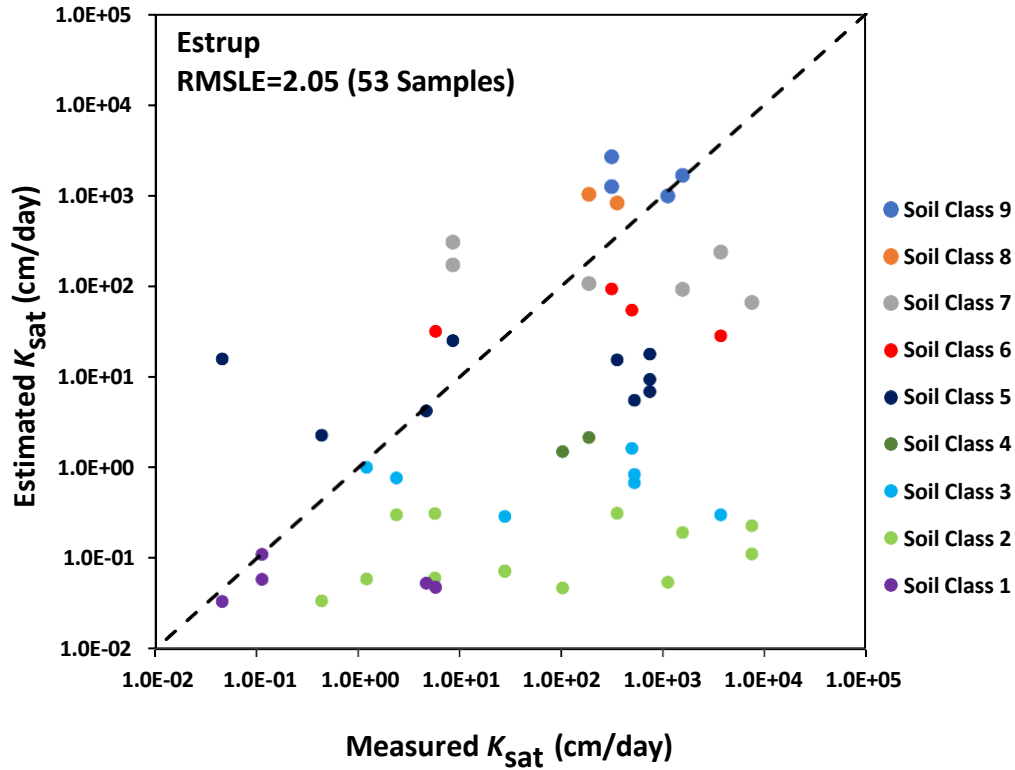
Figure 4.7 The estimated saturated hydraulic conductivity at the large scale against the measured one for samples in the Estrup site. The solid line indicates the 1:1 line.

4.3 -Limitations

The K_{sat} underestimation is probably because the lowest tension head on the SWRC was $h = 10$ cm H_2O. This means some large pores corresponding to tension heads less than 10 cm H_2O were not captured, although they effectively contributed to K_{sat} and its value. We also assumed that the pore-throat radius distribution and typical pore-throat length do not significantly vary with the scale. Such an assumption was required because unfortunately the SWRC measurements as well as pore-throat length data were not available at the large scale in this study. Results of Tinni et al. (2012), Chen et al. (2015), and Shu et al. (2020) on rocks, however, show that $f(r_t)$ may change from one scale to another. For example, Tinni et al. (2012)

measured pore-throat size distributions of several shale samples (Haynesville 1, Haynesville 3, and Pyrophyllite) using particles of different sizes i.e., 0.725, 1.58, 3.5, and 5.68 mm. They found similar pore-throat size distributions derived from different particle sizes for samples Haynesville 1 and Haynesville 3. However, the pore-throat size distribution determined from particle of size 0.725 mm on Pyrophyllite was substantially different from the rest.

Results and calculated RMSLE values presented in Figs. 4.4-4.7 demonstrate that Eq. (3) estimates the K_{sat} at the large scale from the K_{sat} and SWRC measured at the small scale in coarse-textured soils more reliably than that in fine-textured soils. Recall that the soils from Silstrup and Estrup are finer in texture and more structured compared to those from Jyndevad and Tylstrup (Table 3.1). As stated earlier, Eq. (2) only includes the effect of critical pore-throat radius. However, theoretically, K_{sat} depends not only on the value of critical pore-throat radius, but also on electrical conductivity or formation factor (Katz and Thompson, 1986; Ghanbarian, 2020). Therefore, one should expect more accurate estimations, if soil water retention and electrical conductivity data both are available across scales.

Since Eq. (2) does not take into account the effect of electrical conductivity, Esmaeilpour et al. (2021) argued that the relationship between K_{sat} and r_{tc} may not perfectly follow the quadratic relationship. They accordingly generalized such a relationship by replacing the power 2 in Eq. (2) with an optimized exponent. For their simulated pore networks, Esmaeilpour et al. (2021) found an exponent of 3.03 instead of 2. By comparing with pore-scale simulations, they showed that Eq. (2) with the generalized exponent yielded more accurate estimations than the exponent 2. The exponent 2 is a reasonable choice for the Jyndevad and Tylstrup sites with coarser soil textures. It is also close to 2.22, the experimental exponent reported by (Ghanbarian and Skaggs, 2022) for coarse-textured soil samples from the GRIZZLY database. One may,

however, need an exponent greater than 2 to improve the large-scale K_{sat} estimations for the Silstrup and Estrup sites with finer soil textures.

In this study, we estimated the K_{sat} at the large scale (6280 cm^3) from the K_{sat} and SWRC measured at the small scale (100 cm^3). This was required because the Iversen et al. (2001) dataset did not include porosity or SWRC at the larger scale. Since within the critical path analysis framework K_{sat} depends on both critical pore-throat radius and electrical conductivity, further investigations are required to evaluate the accuracy and reliability of Eqs. (2)-(4) using a large database including samples of various textural properties with SWRC, electrical conductivity, and K_{sat} measured at difference scales.

Chapter 5 - Conclusion

Understanding the effect of scale on hydraulic and physical properties of soils has been challenging in soil science and hydrology. In this study, we used concepts from percolation theory and critical path analysis to estimate the K_{sat} at the large scale (6280 cm^3) from soil water retention curve and saturated hydraulic conductivity measured at the small scale (100 cm^3). To evaluate the proposed approach, we used 196 soil samples collected from different horizons and sites in Denmark. We first adapted a classification technique widely used in petroleum engineering and grouped soils using the porosity and permeability measurements available at the small scale. We detected nine soil classes with average flow zone indicator spanned from 0.05 μm in class 1 to 9 μm in class 9. Using the proposed model, we then estimated the K_{sat} at the large scale from the K_{sat} and SWRC measured at the small scale. By comparison with experiments, we found RMSLE = 0.45 (cm/day) for the Jyndevad site with 73 samples, 0.77 (cm/day) for the Tylstrup site with 25 samples, 1.90 (cm/day) for the Silstrup site with 45 samples, and 2.05 (cm/day) for the Estrup with 53 samples. We discussed that although the estimations were reasonable, for higher accuracy one needs to collect electrical conductivity and soil water retention data consistently at all scales. This is because based on critical path analysis K_{sat} not only depends on critical pore-throat radius but also electrical conductivity. Further investigations are required to evaluate the proposed model using a broader type of soils with various levels of heterogeneity.

Chapter 6 - Reference

Adeyemi, B., Ghanbarian, B., Winter, C.L., King, P.R., 2022. Determining effective
permeability at reservoir scale: Application of critical path analysis. Adv. Water Resour.
159. https://doi.org/10.1016/j.advwatres.2021.104096

Amaefule, J.O., Altunbay, M., Tiab, D., Kersey, D.G., Keelan, D.K., 1993. Enhanced reservoir
description: using core and log data to identify hydraulic (flow) units and predict
permeability in uncored intervals/wells, in: SPE Annual Technical Conference and
Exhibition, Houston, Texas. p. SPE-26436-MS.

Aslannejad, H., Hassanizadeh, S.M., Raoof, A., de Winter, D.A.M., Tomozeiu, N., van
Genuchten, M.T., 2017. Characterizing the hydraulic properties of paper coating layer using
FIB-SEM tomography and 3D pore-scale modeling. Chem. Eng. Sci. 160, 275–280.
https://doi.org/10.1016/j.ces.2016.11.021

Bear, J., Braester, C., 1972. On the Flow of Two Immscible Fluids in Fractured Porous Media.
Dev. Soil Sci. 2, 177–202. https://doi.org/10.1016/S0166-2481(08)70538-5

Bhattacharya, S., Byrnes, A.P., Watney, W.L., Doveton, J.H., 2008. Flow unit modeling and
fine-scale predicted permeability validation in Atokan sandstones: Norcan East field,
Kansas. Am. Assoc. Pet. Geol. Bull. 92, 709–732.

Bölscher, T., Koestel, J., Etana, A., Ulén, B., Berglund, K., Larsbo, M., 2021. Changes in pore
networks and readily dispersible soil following structure liming of clay soils. Geoderma
390. https://doi.org/10.1016/j.geoderma.2021.114948

Brunetti, G.F.A., De Bartolo, S., Fallico, C., Frega, F., Rivera Velásquez, M.F., Severino, G.,
2022. Experimental investigation to characterize simple versus multi scaling analysis of
hydraulic conductivity at a mesoscale. Stoch. Environ. Res. Risk Assess. 36, 1131–1142.

https://doi.org/10.1007/s00477-021-02079-w

Chen, Y., Wei, L., Mastalerz, M., Schimmelmann, A., 2015. The effect of analytical particle size
on gas adsorption porosimetry of shale. Int. J. Coal Geol. 138, 103–112.
https://doi.org/10.1016/j.coal.2014.12.012

De Smedt, F., Wauters, F., Sevilla, J., 1986. Study of tracer movement through unsaturated sand.
Geoderma 38, 223–236.

Dexter, A.R., 2004. Soil physical quality: Part I. Theory, effects of soil texture, density, and
organic matter, and effects on root growth. Geoderma 120, 201–214.
https://doi.org/10.1016/j.geoderma.2003.09.004

Division, U.S.D. of A.S.S., Survey, U.S.D. of S., 1993. Soil survey manual. US Department of
Agriculture.

Elliot, T.R., Reynolds, W.D., Heck, R.J., 2010. Use of existing pore models and X-ray computed
tomography to predict saturated soil hydraulic conductivity. Geoderma 156, 133–142.
https://doi.org/10.1016/j.geoderma.2010.02.010

Esmaeilpour, M., 2021. Scale-Dependent petrophysical properties in porous media: A pore-
network study. MSc thesis. Kansas State University.

Esmaeilpour, Misagh, Ghanbarian, B., Liang, F., Liu, H., 2021. Scale-dependent permeability
and formation factor in porous media : Applications of percolation theory. Fuel 301,
121090. https://doi.org/10.1016/j.fuel.2021.121090

Esmaeilpour, M., Ghanbarian, B., Liang, F., Liu, H.H., 2021. Scale-dependent permeability and
formation factor in porous media: Applications of percolation theory. Fuel 301, 121090.

Fallico, C., De Bartolo, S., Troisi, S., Veltri, M., 2010. Scaling analysis of hydraulic conductivity
and porosity on a sandy medium of an unconfined aquifer reproduced in the laboratory.

Geoderma 160, 3–12.

Fallico, C., Vita, M.C., Bartolo, S. De, Straface, S., 2012. in a Confined Aquifer 385–391.

Freeze, R.A., Cherry, J.A., 1979. Groundwater. Prentice-Hall.

Gao, G., Zhan, H., Feng, S., Fu, B., Huang, G., 2012. A mobile-immobile model with an asymptotic scale-dependent dispersion function. J. Hydrol. 424–425, 172–183. https://doi.org/10.1016/j.jhydrol.2011.12.041

Garbesi, K., Sextro, R.G., Robinson, A.L., Wooley, J.D., Owens, J.A., Nazaroff, W.W., 1996. Scale dependence of soil permeability to air: Measurement method and field investigation. Water Resour. Res. 32, 547–560.

Genuchten, V., Nielsen, D., 1986. Describing and predicting the hydraulic properties of unsaturated soils. Int. J. Rock Mech. Min. Sci. Geomech. Abstr. https://doi.org/10.1016/0148-9062(86)91047-8

Ghanbarian-Alavijeh, B., Liaghat, A., Huang, G.H., van Genuchten, M.T., 2010. Estimation of the van Genuchten Soil Water Retention Properties from Soil Textural Data. Pedosphere 20, 456–465. https://doi.org/10.1016/S1002-0160(10)60035-5

Ghanbarian, B., 2022a. Scale dependence of tortuosity and diffusion: Finite-size scaling analysis. J. Contam. Hydrol. 245, 103953.

Ghanbarian, B., 2022b. Estimating the scale dependence of permeability at pore and core scales: Incorporating effects of porosity and finite size. Adv. Water Resour. 161, 104123.

Ghanbarian, B., 2020. Applications of critical path analysis to uniform grain packings with narrow conductance distributions: I. Single-phase permeability. Adv. Water Resour. 137, 103529. https://doi.org/10.1016/j.advwatres.2020.103529

Ghanbarian, B., Esmaeilpour, M., Ziff, R.M., Sahimi, M., 2021. Effect of Pore-Scale

Heterogeneity on Scale-Dependent Permeability: Pore-Network Simulation and Finite-Size

Scaling Analysis. Water Resour. Res. 57, 1–38. https://doi.org/10.1029/2021WR030664

Ghanbarian, B., Hunt, A.G., Sahimi, M., Ewing, R.P., Skinner, T.E., 2013. Percolation Theory

Generates a Physically Based Description of Tortuosity in Saturated and Unsaturated

Porous Media. Soil Sci. Soc. Am. J. 77, 1920. https://doi.org/10.2136/sssaj2013.01.0089

Ghanbarian, B., Skaggs, T.H., 2022. Soil water retention curve inflection point: Insight into soil

structure from percolation theory. Soil Sci. Soc. Am. J. 86, 338–344.

https://doi.org/10.1002/saj2.20360

Ghanbarian, B., Taslimitehrani, V., Dong, G., Pachepsky, Y.A., 2015. Sample dimensions effect

on prediction of soil water retention curve and saturated hydraulic conductivity. J. Hydrol.

528, 127–137. https://doi.org/10.1016/j.jhydrol.2015.06.024

Ghanbarian, B., Taslimitehrani, V., Pachepsky, Y.A., 2017. Accuracy of sample dimension-

dependent pedotransfer functions in estimation of soil saturated hydraulic conductivity.

Catena 149, 374–380. https://doi.org/10.1016/j.catena.2016.10.015

Godoy, V.A., Zuquette, L.V., Gómez-Hernández, J.J., 2019. Spatial variability of hydraulic

conductivity and solute transport parameters and their spatial correlations to soil properties.

Geoderma 339, 59–69. https://doi.org/10.1016/j.geoderma.2018.12.015

Guimerà, J., Vives, L., Carrera, J., 1995. A discussion of scale effects on hydraulic conductivity

at a granitic site (El Berrocal, Spain). Geophys. Res. Lett. 22, 1449–1452.

https://doi.org/10.1029/95GL01493

Heijs, A.W.J., de Lange, J., Schoute, J.F.T., Bouma, J., 1995. Computed tomography as a tool

for non-destructive analysis of flow patterns in macroporous clay soils. Geoderma 64, 183–

196. https://doi.org/10.1016/0016-7061(94)00020-B

Hopmans, J.W., Nielsen, D.R., Bristow, K.L., 2002. How useful are small-scale soil hydraulic property measurements for large-scale vadose zone modeling? Geophys. Monogr. Ser. 129, 247–258. https://doi.org/10.1029/129GM20

Hunt, A., Ewing, R., Ghanbarian, B., 2014. Percolation theory for flow in porous media. Springer.

Hunt, A.G., 2006. Scale-dependent hydraulic conductivity in anisotropic media from dimensional cross-over. Hydrogeol. J. 14, 499–507. https://doi.org/10.1007/s10040-005-0453-6

Iversen, B. V., Lamandé, M., Torp, S.B., Greve, M.H., Heckrath, G., De Jonge, L.W., Moldrup, P., Jacobsen, O.H., 2012. Macropores and macropore transport: Relating basic soil properties to macropore density and soil hydraulic properties. Soil Sci. 177, 535–542. https://doi.org/10.1097/SS.0b013e31826dd155

Iversen, B. V., Moldrup, P., Schjønning, P., Loll, P., 2001. Air and water permeability in differently textured soils at two measurement scales. Soil Sci. 166, 643–659.

Jarvis, N., 2008. Near-Saturated Hydraulic Properties of Macroporous Soils. Vadose Zo. J. 7, 1302–1310. https://doi.org/10.2136/vzj2008.0065

Javaux, M., Vanclooster, M., 2006. Scale-dependency of the hydraulic properties of a variably saturated heterogeneous sandy subsoil. J. Hydrol. 327, 376–388.

Jiménez-Aguirre, M.T., Isidoro, D., Usón, A., 2018. Soil variability in La Violada Irrigation District (Spain): II Characterizing hydrologic and salinity features. Geoderma 311, 67–77. https://doi.org/10.1016/j.geoderma.2017.04.024

Katz, A.J., Thompson, A.H., 1986. Quantitative prediction of permeability in porous rock. Phys. Rev. B 34, 8179–8181.

Klute, A., Dirksen, C., 2018. Hydraulic conductivity and diffusivity: Laboratory methods. Methods Soil Anal. Part 1 Phys. Mineral. Methods 9, 687–734. https://doi.org/10.2136/sssabookser5.1.2ed.c28

Klute, A., Dirksen, C., 1986. Hydraulic conductivity and diffusivity: Laboratory methods. Methods Soil Anal. Part 1 Phys. Mineral. Methods 9, 687–734. https://doi.org/10.2136/sssabookser5.1.2ed.c28

Koestel, J., Larsbo, M., Jarvis, N., 2020. Scale and REV analyses for porosity and pore connectivity measures in undisturbed soil. Geoderma. https://doi.org/10.1016/j.geoderma.2020.114206

Kogut, P.M., Straley, J.P., 1979. Distribution-induced non-universality of the percolation conductivity exponents. J. Phys. C Solid State Phys. 12, 2151–2159. https://doi.org/10.1088/0022-3719/12/11/023

Lauren, J.G., Wagnet, R.J., Bouma, J., Wosten, J.H.M., 1988. Variability of saturated hydraulic conductivity in a Glossaquic Hapludalf with macropores. Soil Sci. 145, 20–28.

Martin, A.J., Solomon, S.T., Hartmann, D.J., 1997. Characterization of petrophysical flow units in carbonate reservoirs. Am. Assoc. Pet. Geol. Bull. 81, 734–759.

Matyka, M., Khalili, A., Koza, Z., 2008. Tortuosity-porosity relation in porous media flow. Phys. Rev. E - Stat. Nonlinear, Soft Matter Phys. 78, 1–8. https://doi.org/10.1103/PhysRevE.78.026306

Minasny, B., McBratney, A.B., Salvador-Blanes, S., 2008. Quantitative models for pedogenesis - A review. Geoderma 144, 140–157. https://doi.org/10.1016/j.geoderma.2007.12.013

Molz, F.J., Rajaram, H., Lu, S., 2004. Stochastic fractal-based models of heterogeneity in subsurface hydrology: Origins, applications, limitations, and future research questions. Rev.

Geophys. 42, 1–42. https://doi.org/10.1029/2003RG000126

Mostaghimi, P., Blunt, M.J., Bijeljic, B., 2013. Computations of Absolute Permeability on
Micro-CT Images. Math. Geosci. 45, 103–125. https://doi.org/10.1007/s11004-012-9431-4

Pachepsky, Y., Hill, R.L., 2017. Scale and scaling in soils. Geoderma 287, 4–30.
https://doi.org/10.1016/j.geoderma.2016.08.017

Pachepsky, Y.A., Guber, A.K., Yakirevich, A.M., McKee, L., Cady, R.E., Nicholson, T.J., 2014.
Scaling and Pedotransfer in Numerical Simulations of Flow and Transport in Soils. Vadose
Zo. J. 13, vzj2014.02.0020. https://doi.org/10.2136/vzj2014.02.0020

Sahimi, M., Hughes, B.D., Scriven, L.E., Davis, H.T., 1986. Dispersion in flow through porous
media-I. One-phase flow. Chem. Eng. Sci. 41, 2103–2122. https://doi.org/10.1016/0009-
2509(86)87128-7

Sánchez-Vila, X., Carrera, J., Girardi, J.P., 1996. Scale effects in transmissivity. J. Hydrol. 183,
1–22.

Schulze-Makuch, D., 1996. Facies dependent scale behavior of hydraulic conductivity and
longitudinal dispersivity in the carbonate aquifer of Southeastern Wisconsin, Ph.D.
dissertation, University of Wisconsin, Milwaukee.

Schulze-Makuch, D., Carlson, D.A., Cherkauer, D.S., Malik, P., 1999. Scale dependency of
hydraulic conductivity in heterogeneous media. Ground Water 37, 904–919.

Shu, Y., Xu, Y., Jiang, S., Zhang, L., Zhao, X., Pan, Z., Blach, T.P., Sun, L., Bai, L., Hu, Q.,
Sun, M., 2020. Effect of particle size on pore characteristics of organic-rich shales:
Investigations from small-angle neutron scattering (sans) and fluid intrusion techniques.
Energies 13. https://doi.org/10.3390/en13226049

Tinni, A., Fathi, E., Agarwal, R., Sondergeld, C., Akkutlu, Y., Rai, C., 2012. Shale permeability

measurements on plugs and crushed samples. Soc. Pet. Eng. - SPE Can. Unconv. Resour. Conf. 2012, CURC 2012 1, 342–355. https://doi.org/10.2118/162235-ms

Tyč, S., Halperin, B.I., 1989. Random resistor network with an exponentially wide distribution of bond conductances. Phys. Rev. B 39, 877–880. https://doi.org/10.1103/PhysRevB.39.877

van Genuchten, M.T., 1980. A closed-form equation for predicting the hydraulic conductivity of unsaturated soils. Soil Sci. Soc. Am. J. 44, 892–898.

Younes, A., Fahs, M., Ataie-Ashtiani, B., Simmons, C.T., 2020. Effect of distance-dependent dispersivity on density-driven flow in porous media. J. Hydrol. 589, 125204. https://doi.org/10.1016/j.jhydrol.2020.125204

Zakizadeh Abkenar, F., Rasoulzadeh, A., 2019. Functional Evaluation Of Pedotransfer Functions For Simulation Of Soil Profile Drainage. Irrig. Drain. 68, 573–587. https://doi.org/10.1002/ird.2328

Zota, A.R., Willis, R., Jim, R., Norris, G.A., Shine, J.P., Duvall, R.M., Schaider, L.A., Spengler, J.D., 2009. Impact of mine waste on airborne respirable particulates in Northeastern Oklahoma, United States. J. Air Waste Manag. Assoc. 59, 1347–1357. https://doi.org/10.3155/1047-3289.59.11.1347

Appendix A - Large-scale K_{sat} Estimation Script

This script reads soil retention curve data and determines optimized Van Genuchten parameters such as α, *n*, and *m.* Afterwards large-scale K_{sat} estimations are generated using the method described above. Data is read in .mat files using MATLAB.

```matlab
Ksat_large = xlsread('JK_Danish_Final.xlsx',4,'C16:BW16');
Ksat_small = xlsread('JK_Danish_Final.xlsx',4,'C17:BW17');

ns = length(Ksat_large);                    %number of samples

h = xlsread('JK_Danish_Final.xlsx',4,'A6:A13');
theta = xlsread('JK_Danish_Final.xlsx',4,'C6:BW13');

%Fitting the vG model to all samples
for i = 1:1:ns

    Qs(i) = theta(1,i);

    %Initial guess vector: theta_r, alpha, n, and m
    x0 = [theta(end,i) 0.1 3.5 1-1/3.5];

    %Fit options including lower and upper bounds
    fo = fitoptions('Method', 'NonlinearLeastSquares','lower',[0 0 1
0],'upper',[theta(end,i) 10 100 1-1/100]);

    fitfun = fittype( @(theta_r,a,n,m,x) (Qs(i) - theta_r).*(1+(a.*x).^n).^(-
m),'options',fo );

    [fitted_curve,gof] = fit(h,theta(:,i),fitfun,'StartPoint',x0,'robust','LAR')

    % Save the coeffiecient values
    coeffvals = coeffvalues(fitted_curve);
    Qr(i) = coeffvals(1);
    A(i) = coeffvals(2);
    N(i) = coeffvals(3);
    M(i) = coeffvals(4);
end

r=0.149./h;
r_min = 0.149./max(h);
r_max = 0.149./h(2);

d_small = 6.1;                    %internal diameter in cm
d_large = 20;                     %internal diameter in cm
V_small = 100;                    %small sample volume
V_large = 6280;                   %large sample volume
l_small = (V_small)/(pi/4*d_small^2);     %length determined from volume and internal
diameter
l_large = (V_large)/(pi/4*d_large^2);     %length determined from volume and internal
diameter
L_small = (V_small)^(1/3);        %equivalent length determined from volume
```

```matlab
L_large = (V_large)^(1/3);       %equivalent length determined from volume

for i = 1:1:ns
    theta_s = Qs(i);
    theta_r = Qr(i);
    a = A(i);
    n = N(i);
    m = M(i);
    h_inf = (1/a)*(1/m)^(1/n);

    %inline function for the vG model with x representing matric potential
    vG = @(x) (theta_s - theta_r).*(1+(a.*x).^n).^(-m) + theta_r;

    %inline function for the pore size distribution derived from vG model with x
representing pore radius
    f_r = @(x) (m*n)*(theta_s - theta_r).*(a.*0.149./x).^n.*(1+(a.*0.149./x).^n).^(-
m-1);
    r3f_r = @(x) x.^2.*(m*n).*(theta_s -
theta_r).*(a.*0.149./x).^n.*(1+(a.*0.149./x).^n).^(-m-1);

    funsat1 = @(x) integral(r3f_r,x,r_max) - vG(15000)/theta_s .*
integral(r3f_r,r_min,r_max);
    r_crit_sat_small(i) = fzero(funsat1,r_max);

    l0_sat(i) =
(integral(r3f_r,r_crit_sat_small(i),r_max)/integral(r3f_r,r_min,r_max) * L_small) /
(1 - (integral(r3f_r,r_crit_sat_small(i),r_max)/integral(r3f_r,r_min,r_max))^0.88);

    funsat2 = @(x) integral(r3f_r,x,r_max)./integral(r3f_r,r_min,r_max) -
(l0_sat(i)/(L_large+l0_sat(i)))^(1/0.88);
    r_crit_sat_large(i) = fzero(funsat2,r_max);


end

x = linspace(0.001,100000,ns);
y = linspace(0.001,100000,ns);
figure
loglog(x, y, 'r-')
hold on

%Plotting the estimated sat hyd con vs the measured value
Ksat_large_est = Ksat_small .* (r_crit_sat_large./r_crit_sat_small).^2;
%loglog(Ksat_large,Ksat_large_est,'ok',Ksat_large,Ksat_small,'*r');
loglog(Ksat_large,Ksat_large_est,'ok','MarkerFaceColor','k');

%Calculating root mean log-transformed error (RMSLE)
sum_sat_large = sum((log10(Ksat_large)-log10(Ksat_large_est)).^2);
RMSLE_sat_large = sqrt(sum_sat_large/length(Ksat_large))
sum_sat_small = sum((log10(Ksat_large)-log10(Ksat_small)).^2);
RMSLE_sat_small = sqrt(sum_sat_small/length(Ksat_large))

xlabel('Measured large scale K_{sat} [cm/day]')
ylabel('Estimated large scale K_{sat} [cm/day]')
axis ([0.01 100000 0.01 100000])
```

```matlab
% title('Jyndevad: RMSLE=0.45 with 73 samples')
text(0.01615,65000,'Jyndevad','FontSize',9,'FontWeight','bold','Color','k')
text(0.01615,35000,'RMSLE=0.45 (73
Samples)','FontSize',9,'FontWeight','bold','Color','k')
```